ACS OMEGA

Open Access

http://pubs.acs.org/journal/acsodf

Article

Polypyrrole Coating via Lemieux-von Rudloff Oxidation on Magnetite Nanoparticles for Highly Efficient Removal of Chromium(VI) from Wastewater

Published as part of ACS Omega virtual special issue "Magnetic Nanohybrids for Environmental Applications".

Md. Kawsar Hossain, Md. Mehadi Hasan, Md. Shahidul Islam, O. Thompson Mefford, Hasan Ahmad, and Md. Mahbubor Rahman*

Cite This: *ACS Omega* 2024, 9, 19077−19088

Read Online

ACCESS | Metrics & More | Article Recommendations

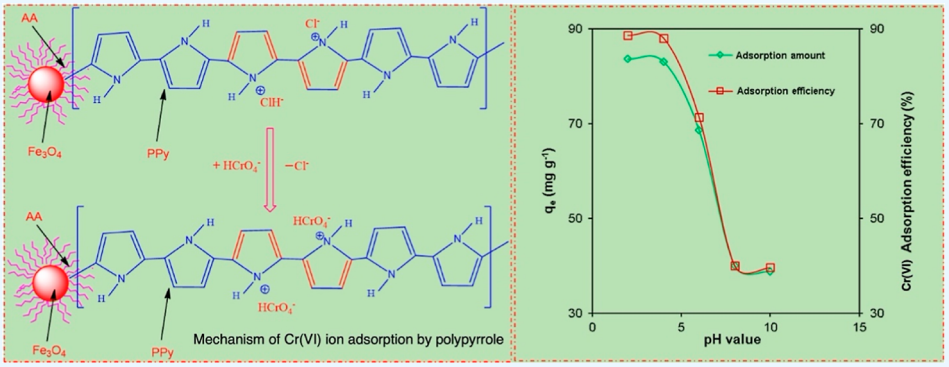

ABSTRACT: An alternative way for the coating of polypyrrole (PPy) polymer on hydrophobic magnetite (Fe_3O_4) nanoparticles is reported here to capture toxic chromium ions, Cr (VI), present in water. Iron oxide magnetic nanoparticles (Fe_3O_4) were synthesized by the conventional coprecipitation technique using $FeCl_3·6H_2O$ and $FeSO_4·7H_2O$ iron precursors and subsequently modified with oleic acid (OA). Then OA-Fe_3O_4 hydrophobic nanoparticles were oxidized using the Lemieux-von Rudloff reaction to transfer OA into hydrophilic azelaic acid (AA) ($HOOC(CH_2)_7COOH$-modified magnetic nanoparticles (AA−Fe_3O_4). Finally, a PPy polymer coating was formed by a seeded polymerization of pyrrole, using AA−Fe_3O_4 as seeds. The average size of PPy/Fe_3O_4 nanocomposites is 12.33 nm and is almost spherical in shape. The surface composition is confirmed by FTIR and thermogravimetry analyses. An X-ray diffraction study confirmed the formation of highly crystalline Fe_3O_4 nanoparticles, and the crystallinity was retained after the surface modification. The adsorption study suggested that the Cr(VI) ion adsorption is highly pH-dependent and the maximum amount of adsorption is obtained at pH 2.0. The adsorption results revealed that the Langmuir model provided the best fit for the isotherm, with a maximum adsorption capacity reaching approximately 173.22 mg g^{-1} at 323 K. Spontaneous and endothermic adsorption processes were confirmed by evaluating the thermodynamic parameters obtained in this investigation. The kinetics study showed that the interaction between Cr(VI) ions and magnetic nanocomposites was directed by a pseudo-second-order rate process indicating chemisorption. The prepared PPy/Fe_3O_4 nanocomposites would be promising adsorbents to purify water by eliminating Cr(VI) metal ions from wastewater.

1. INTRODUCTION

Environmental pollution caused by heavy metals, which are introduced into the environment as nondegradable products from various sources, has become a major health concern because of their toxic bioaccumulative nature.[1,2] Several kinds of toxic metal ions, for example, Cu(II), Cd(II), As(II), Hg(II), and Cr(VI), among others, have been observed in wastewater.[3] Important for the research reported here, chromium ions are found in the form of trivalent Cr(III) and hexavalent Cr(VI), while later one is considered as high toxic because of its carcinogenic effects on the skin, lungs, livers, kidneys, and stomach.[4,5] This, its removal from wastewater, is critical for our safety of human beings. Among

Received: December 10, 2023
Revised: March 28, 2024
Accepted: April 10, 2024
Published: April 22, 2024

Scheme 1. Schematic Illustration for Synthesis of PPy/Fe_3O_4 Nanocomposites[a]

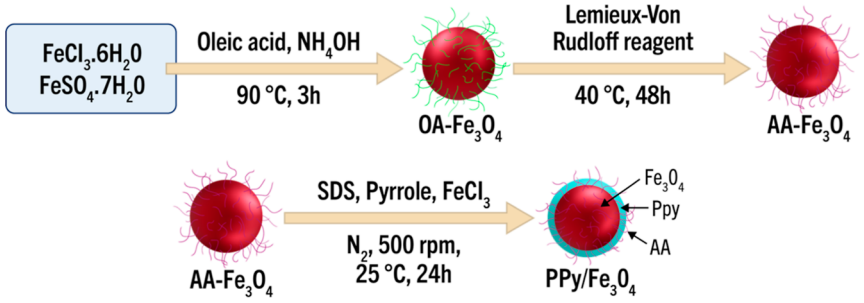

[a]The OA-coated iron oxide magnetite particles (OA−Fe_3O_4) were prepared using a coprecipitation method involving iron salts, followed by coating with an OA coating (Step 1). AA-modified nanoparticles (AA−Fe_3O_4) were obtained using Limeux-Van Rudloff reagents, i.e., oxidizing the C═C bonds of OA (Step 2). Finally, AA−Fe_3O_4 nanoparticles were coated with PPy through the polymerization of the pyrrole.

the different methods[6−11] employed for pollutant removal from wastewater, adsorption methods[12,13] have become a very potential technique because of reusability, low cost, environmental benign and easy handling of adsorbents.

Currently, polyaniline (PAni) and polypyrrole (PPy) are used to separate Cr(VI) ions from the wastewater.[14−18] In addition, nonmagnetic PPy-based composite particles have also been reported for use in water treatment.[19−21] However, time-consuming centrifugation processes and low recovery limit the use of such particles in separation technology. Alternatively, the use of magnetic nanoparticles has the potential to eliminate the time-consuming centrifugation, filtering, and sediment process.[22] In light of this potential, magnetic nanocomposites with a magnetic core are attracting much interest for Cr(VI) ion adsorption because of their easy and fast separation by an external magnet.[23−25] The advantages of using PPy as a coating material for F_3O_4 include (i) the protection of magnetic particles from leaching out and aggregation and (ii) the cationic nature of PPy polymers, making it feasible for both adsorption as well as the reduction of toxic Cr(VI).[26,27] In early research in this area, Chávez-Guajardo et al. synthesized PPy/maghemite and PAni/maghemite magnetic nanocomposites, comparing their effective capturing of Cr(VI) and Cu(II) ions from an aqueous medium.[28] This study confirmed the higher and faster removal of Cr(VI) ions using a PPy conducting polymer compared to the PAni. This study used Fe_3O_4-coated PPy composite particles that were prepared in a multistep reaction, with the fabricated particles successively being used for the removal of Cr(VI) ions up to two adsorption−desorption cycles. In further research, Ahmad et al. investigated chromium ions capture by using conductive stimuli-responsive PPy nanocomposite hydrogel particles as an adsorbent.[29] However, despite the promise of PPy-coated magnetic nanoparticles in these applications, the coating of PPy on Fe_3O_4 remains a challenge because Fe_3O_4 must have functional groups, specifically OH, COOH, to bind the polymer chain of PPy to be adsorbed or immobilized on the Fe_3O_4 nanoparticles. Generally, oleic acid (OA) coated hydrophobic magnetite nanoparticles (OA−Fe_3O_4) need to be further subjected to ligand exchange or surface treatment with amphiphilic polymers to obtain hydrophilic magnetic nanoparticles for PPy coating on Fe_3O_4.

The research reported here introduces a new approach for converting OA-coated Fe_3O_4 hydrophobic nanoparticles to hydrophilic azelaic acid (AA)-modified Fe_3O_4 nanoparticles through a ligand oxidation reaction using the Lemieux-von Rudloff reagent. The conversion of the carbon−carbon double bond of OA at C_9−C_{10} to more polar carboxylic acid groups creates a strong possibility of coupling with PPy. This strong interaction should minimize the leaching out of the PPy shell layer during metal ion capture in water. The chromium ion adsorption performance of the PPy-modified Fe_3O_4 nanocomposites is evaluated in terms of maximum adsorption capacity, adsorption kinetics, isotherms, thermodynamics, and cyclic adsorption. Our results demonstrate both a novel synthesis of Fe_3O_4/PPy nanocomposites and the promising adsorption of metal ions from wastewater for applications in environmental science.

2. EXPERIMENTAL SECTION

2.1. Materials. Ferric chloride hexahydrate ($FeCl_3·6H_2O$) and ferrous sulfate heptahydrate ($FeSO_4·7H_2O$) were purchased from LOBA Chemie, India, and Merk, Germany. OA from Sigma-Aldrich was used, keeping it stored in the refrigerator before use. Sodium dodecyl sulfate (SDS) and pyrrole were from Fluka and Sigma-Aldrich, respectively. 1-Butanol, acetone, ethanol, and cyclohexane were distilled before use, while ammonium hydroxide (NH_4OH), potassium carbonate (K_2CO_3), potassium permanganate ($KMnO_4$), potassium dichromate ($K_2Cr_2O_7$), sodium periodate ($NaIO_4$), and other chemicals were of analytical grade and used as received.

2.2. Methods. *2.2.1. Synthesis of OA Coated Iron Oxide (OA−Fe_3O_4) Nanoparticles.* Iron oxide magnetic (Fe_3O_4) nanoparticles were synthesized by using a coprecipitation reaction of ferrous and ferric salts in ammonium hydroxide solutions. For this synthesis method, 2.43 g of $FeCl_3·6H_2O$ and 1.67 g of $FeSO_4·7H_2O$ were dissolved in 50 mL of water in a 250 mL reactor and heated to 90 °C. Then, 15 mL of ammonium hydroxide was added to the iron solution, and a black precipitate of iron oxide was immediately formed. After 30 min of reaction time for nucleation and growth, 4 mL of OA was added dropwise to the reaction solution. The reaction was continued for 3 h and the black OA-Fe_3O_4 nanoparticles were purified and stored as dry powder for further use.

2.2.2. Oxidation of the OA Chain of OA-Fe_3O_4 through a Lemieux-Von Rudloff Reaction. AA−Fe_3O_4 nanoparticles were prepared using a modified method found in the

https://doi.org/10.1021/acsomega.3c09864
ACS Omega 2024, 9, 19077−19088

literature.[30] Briefly, a reaction mixture was prepared from the presynthesized Fe_3O_4 nanoparticles (0.5 g), cyclohexane (200 mL), butanol-1 (150 mL), DI water (60 mL), and 5% (w/v) potassium carbonate aqueous solution (5 mL). Then 100 mL of Lemieux-Von Rudloff reagents (5.7 mM $KMnO_4$ and 0.105 M $NaIO_4$) was added dropwise, and the mixture was stirred for 48 h at 40 °C. A dark brown solution obtained was subsequently washed with ethanol, acetone, and DI water. Finally, the oxidized OA coated Fe_3O_4 nanoparticles were converted into AA coated Fe_3O_4 and dispersed in DI water.

2.2.3. PPy Coating on Iron Oxide Magnetic (AA−Fe_3O_4) Nanoparticles. AA-modified Fe_3O_4 (0.5 g) particles denoted as AA−Fe_3O_4 were well dispersed in an SDS solution (0.0125 g of SDS in 15 mL of water) using 30 min of sonication. Next, 0.25 g of pyrrole was added to the previous mixture and dissolved by stirring for 30 min. Finally, the polymerization of pyrrole was initiated with $FeCl_3$ (1.45 g), and the reaction conditions were maintained at 500 rpm in a N_2 atmosphere at a temperature of 25 °C. The resulting nanocomposites were purified with water to remove the unreacted pyrrole. The purified PPy/Fe_3O_4 nanocomposites were dispersed in DI water and stored for final applications. The detailed synthesis procedure of the PPy/Fe_3O_4 nanocomposites is shown in Scheme 1.

2.2.4. Characterizations. Transmission electron microscopy (TEM) using a Hitachi 7830 instrument at 120 kV was employed to analyze the size and the size distribution. A PerkinElmer (UK) FTIR-100 spectrophotometer was utilized, with spectra recorded in KBr pellets across the range of 4000−200 cm^{-1} using the deflection mode. Surface structure analysis of the PPy/Fe3O4 nanocomposite particles was carried out using an X-ray diffractometer (Bruker D8 ADVANCE, Germany). Chemical composition was determined with a thermogravimetry analyzer (TGA; Seiko Instruments Inc., Japan, model EXSTAR-6000), measuring weight loss from ambient temperature to 800 °C at a heating rate of 20 °C min^{-1} under a nitrogen atmosphere. Magnetic property was analyzed using a vibrating sample magnetometer (VSM; Micro Sense, model EV9, USA). Additionally, a Shimadzu UV-1650pc double-beam UV−visible spectrophotometer and a Mettler Toledo MP 220 microprocessor pH meter from Switzerland were also employed in this study.

2.2.5. Adsorption Study of Cr (VI) Ions. In a 100 mL stopper glass bottle, 0.005 g of PPy/Fe_3O_4 nanocomposites were mixed with 20 mL of a 25 mg L^{-1} Cr(VI) solution to perform the adsorption of Cr (VI) ions by PPy−Fe_3O_4. The studies were carried out at initial pH values of 2, 4, 6, 8, and 10 for pH-dependent analysis. NaOH or a diluted (0.1 M) HCl solution were used to change the pH levels of the aqueous dispersion media of nanocomposites. For 120 min, the Cr-nanocomposite mixture was magnetically agitated at 200 rpm while keeping the temperature constant at 298 K. The nanocomposites were separated by centrifugation at 10,000 rpm and the use of an external magnet. Thirty mL of solution was taken from the Cr (VI)-containing solution. 1.7 mL of 3 M H_2SO_4 and 2 mL of 0.25% diphenyl carbazide are added and diluted the mixture to 50 mL. Finally, the absorbance was measured using a visible spectrophotometer (SP-300; OPTIMA, Japan) at a wavelength of 540 nm. To carry out the desorption experiment, after adding 30 mL of a 0.5 M NaOH solution, the Cr (VI)-loaded adsorbent was magnetically swirled for a whole day. After the resultant solution was centrifuged, the absorbance of the supernatant was measured to determine the concentration of Cr(VI) ions in the solution.

Adsorbed Cr(VI) at equilibrium, q_e (mg g^{-1}), was determined by Formula 1

$$q_e = (C_o - C_e)V/W \quad (1)$$

where C_o and C_e (mg L^{-1}) are the initial and equilibrium concentrations of Cr(VI) ions in solutions, respectively; V (L) is the volume of the solution; and W (g) is the mass of nanocomposites. Using a fixed amount (0.005 g) of PPy/Fe_3O_4 nanocomposite particles, the equilibrium adsorption studies were conducted by altering the starting Cr(VI) ion concentrations (25, 30, 40, and 50 mg L^{-1}) and temperatures (303, 313, and 323 K).

Three different adsorption models, including Langmuir, Freundlich, and Temkin, were employed to explain the adsorption behavior. The Langmuir isotherm model, which assumes monolayer coverage is represented as

$$C_e/q_e = (1/b)q_{max} + C_e/q_{max} \quad (2)$$

where b (L mg^{-1}) is the Langmuir constant, indicating the energy and affinity of adsorption, and q_{max} (mg g^{-1}) is the theoretical monolayer adsorption capacity. The Freundlich model's linear form, which employs a multilayer adsorption to describe affinities, is expressed as

$$\ln q_e = \ln K_f + 1/n \ln C_e \quad (3)$$

where $1/n$ and K_f (adsorption or distribution coefficients) are the Freundlich constants associated with adsorption intensity and capacity, respectively. The Temkin isotherm is provided in linear form as

$$q_e = B\cdot\ln A_T + B\cdot\ln C_e \quad (4)$$

where B (= RT/b), R, T, and A_T (L mg^{-1}) are the Temkin constant, molar gas constant, absolute temperature (K), and binding constant, respectively. Values of A_T and B were attained by a plot of q_e versus ln C_e, and the thermodynamic parameters free energy (ΔG), enthalpy (ΔH), and entropy (ΔS) were determined using the following equations

$$\ln K_c = \Delta S/R - \Delta H/RT \quad (5)$$

$$\Delta G = \Delta H - T\Delta S \quad (6)$$

where K_c is the thermodynamic equilibrium constant.

2.2.6. Reuse Study of Nanocomposites. The reusability of the prepared PPy/Fe_3O_4 nanocomposites was investigated through repeated adsorption−desorption experiments. After each adsorption experiment, the recovered PPy/Fe_3O_4 nanocomposites were treated with 25 mL of a 0.5 M NaOH solution for 2 h. For 30 min, the adsorbent nanocomposites were treated with 0.2 M HCl in order to reuse the used adsorbent for the subsequent adsorption−desorption cycles.

3. RESULTS AND DISCUSSION

3.1. Synthesis and Surface Functionalization of Magnetic Nanoparticles. The total synthesis route for the preparation of PPy/Fe_3O_4 nanocomposites, shown schematically in Scheme 1, is an easy, conventional coprecipitation method. As soon as NH_4OH was added to the reaction solution, a dark black precipitate of nanoparticles was observed. OA coating on Fe_3O_4 made nanoparticles nonpolar and hydrophobic. AA-modified nanoparticles (AA−Fe_3O_4)

https://doi.org/10.1021/acsomega.3c09864
ACS Omega 2024, 9, 19077−19088

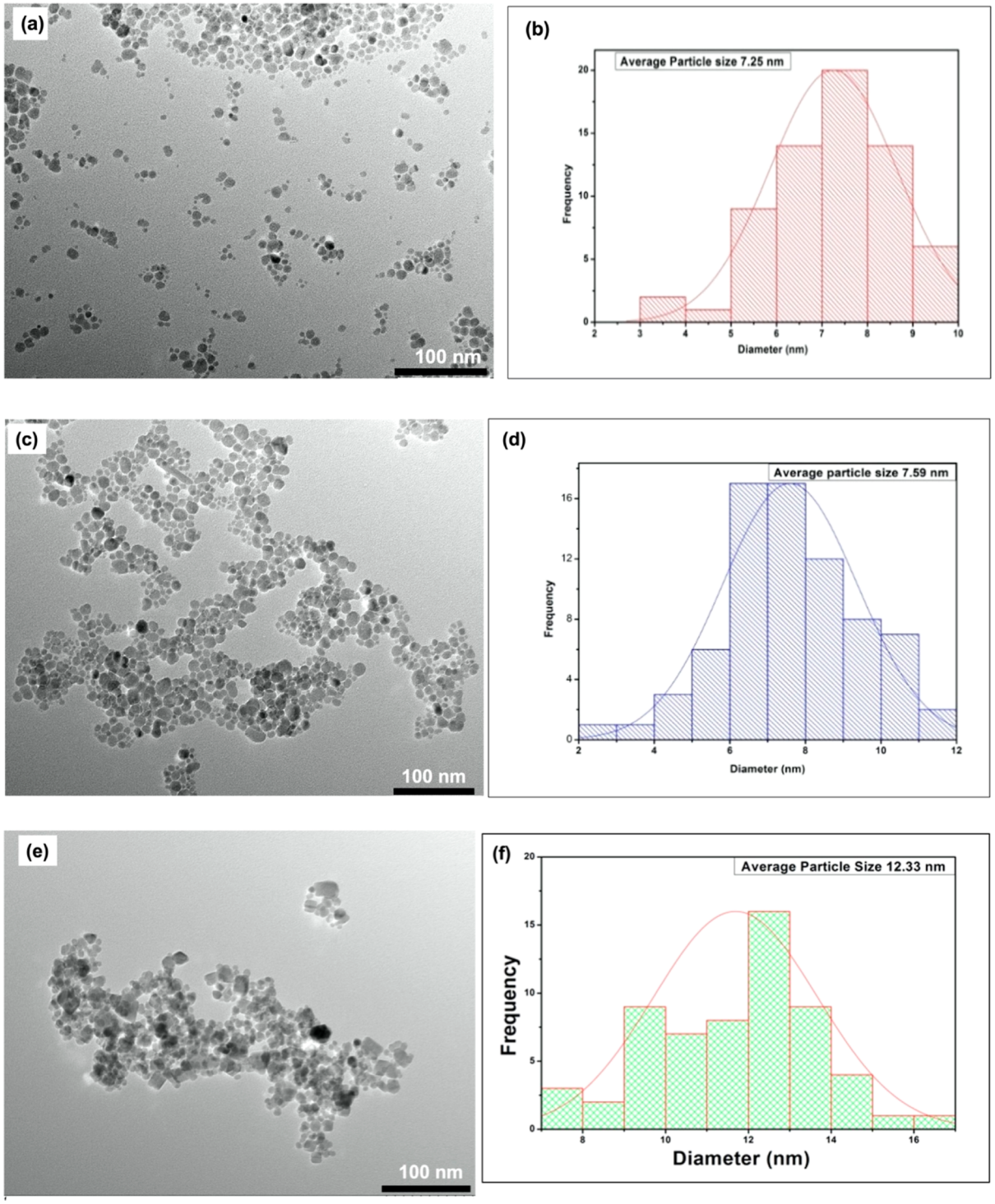

Figure 1. TEM images and corresponding size histograms of the OA−Fe_3O_4 (a,b), AA−Fe_3O_4 (c,d), and PPy/Fe_3O_4 (e,f) nanocomposites.

were then obtained using Limeux-Van Rudloff reagents, i.e., via oxidizing the C═C bonds of OA, which was finally coated with PPy through the seeded oxidative polymerization of pyrrole to obtain the nanocomposites, PPy/Fe_3O_4. The dispersion of the latter two turned the water brownish black.

The TEM images and corresponding size histograms of OA−Fe_3O_4, AA−Fe_3O_4 and PPy/Fe_3O_4 are shown in Figure 1. Regardless of their chemical composition, the magnetic particles are in the nanoscale domain. Both the OA−Fe_3O_4 and AA−Fe_3O_4 nanoparticles are stable, even in the dried state, and individual particles are discernible with clear boundaries. Comparatively, the image of the PPy coated magnetic nanoparticles, PPy/Fe_3O_4 (Figure 2e), indicates the presence of closely packed individual nanoparticles with a probable tendency for aggregation. This behavior is due to the transition of the hydrophilic character of AA-modified nanoparticles (AA−Fe_3O_4) to a more hydrophobic one following modification with the PPy layer. The particles are primarily spherical and polydispersed. The average size of the PPy/Fe_3O_4 (12.33 nm) nanocomposites is slightly larger than those

https://doi.org/10.1021/acsomega.3c09864
ACS Omega 2024, 9, 19077−19088

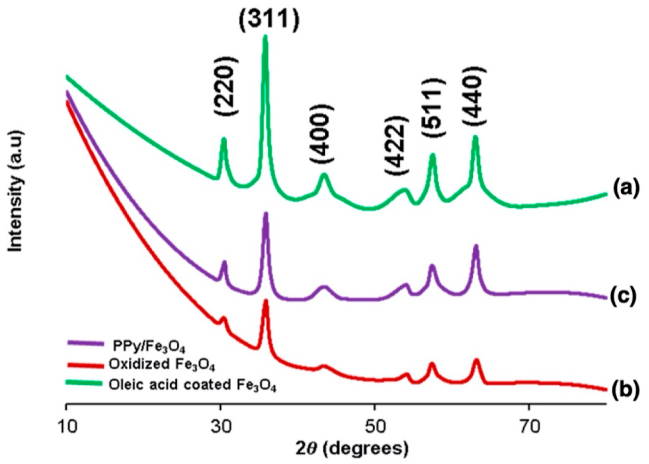

Figure 2. XRD patterns of (a) OA−Fe_3O_4, (b) AA−Fe_3O_4, and (c) PPy/Fe_3O_4 nanoparticles.

of the OA−Fe_3O_4 (7.25 nm) and AA−Fe_3O_4 (7.59 nm) nanoparticles due to the PPy coating on the AA−Fe_3O_4 nanoparticles. This difference also committed the binding of the PPy layer onto AA−Fe_3O_4 nanoparticles. The difference in average size between the OA−Fe_3O_4 and the AA−Fe_3O_4 (Figure 1b,d) nanoparticles is negligible.

The X-ray diffraction (XRD) analysis confirmed both the existence and structure of iron oxide nanoparticles. In Figure 2, the XRD pattern and a noticeable magnetite characteristic peak can be observed at the 2θ value of 35.7°, with some additional peaks at 30.3, 43.1, 53.6, 57.4, and 62.6°, matching, in terns, the planes (311), (220), (400), (422), (511), and (440), respectively. This observation is seen for surface-modified AA−Fe_3O_4 and polymer-coated PPy/Fe_3O_4. The resultant XRD pattern was compared and matched to the JCPDS reference code-75-0449, a pattern referring to the crystal faces of the Fe_3O_4 structure. These results suggested that the peak positions remained the same, but the intensity changed slightly for the surface-modifying PPy coated Fe_3O_4 nanoparticles. The crystalline structure of the Fe_3O_4 nanoparticles is essentially retained, even after surface modification.

Figure 3 shows the FTIR spectra of the OA−Fe_3O_4, AA−Fe_3O_4 and PPy/Fe_3O_4 nanoparticles. A broad peak from 635 to 555 cm^{-1} represents the Fe−O vibration of the magnetic core, indicating not only the formation of Fe_3O_4 but also some

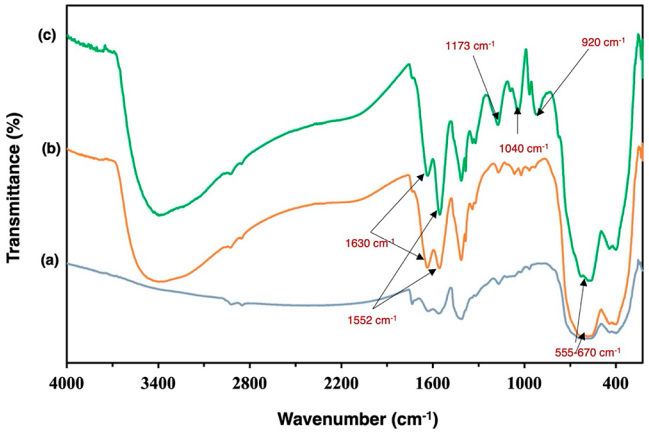

Figure 3. FT-IR spectra of (a) OA−Fe_3O_4, (b) AA−Fe_3O_4, and (c) PPy/Fe_3O_4 nanoparticles.

other forms of iron oxide, such as maghemite and iron oxyhydroxide.[31,32] Two new bands appeared at 1552 and 1630 cm^{-1}, both of which are characteristic of the asymmetric (V_{as}) and symmetric (V_s) stretching vibrations of the carboxylic group of the bond of OA.[33,34] The transmission bands at 2920−2850 cm^{-1} in the OA−Fe_3O_4 nanoparticles (a) are attributed to the asymmetric (V_{as}) and symmetric (V_s) stretching vibrations of methylene (CH_2) in a long alkyl chain.[35] However, in the oxidized AA-Fe_3O_4 nanoparticles (Figure 3b), the bands observed at 1638 and 1556 cm^{-1} indicate the presence of carboxylic groups.

This effect could be a consequence of a combination of molecules bonded symmetrically and molecules bound at an angle to the surface of the carboxylic acids on the nanoparticles' surface. These findings demonstrated that OA was chemisorbed as a carboxylate onto Fe_3O_4 nanoparticles. In the spectrum of the PPy/Fe_3O_4 nanospheres (Figure 3c), the distinctive peaks at 1552 and 1470 cm^{-1} attribute to stretching vibrations of the C═C and C−N bonds of PPy.[36] The peaks at 1318 and 1166 cm^{-1} ascribe to the C−H in-plane vibration, and the peaks at 1040 and 920 cm^{-1} represent the C−H in-plane bending and the ring deformation, respectively.[37,38] The wide band at 781 cm^{-1} is linked to the bending mode of Fe−O−H corresponding to Fe_3O_4, while the absorption bands at 565 cm^{-1} are related to the lattice vibrations of the FeO_6 octahedral.

The inclusion of the inorganic Fe_3O_4 component in the PPy polymer matrix was estimated based on the percentage of weight loss found in the TGA thermograms presented in Figure 4. As this figure shows, both OA−Fe_3O_4 nanoparticles

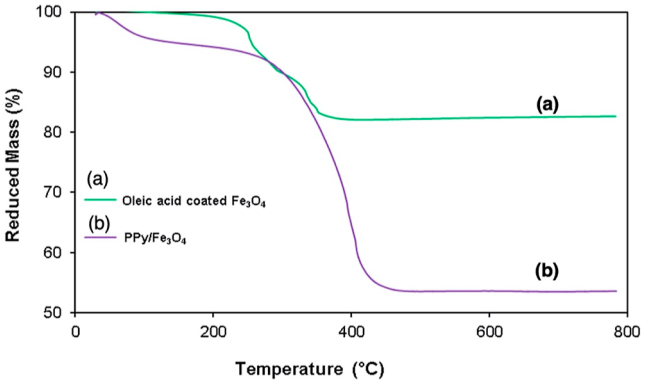

Figure 4. Thermograms of (a) magnetic nanoparticles coated with OA (OA−Fe_3O_4) and (b) magnetic PPy nanocomposites (PPy/Fe_3O_4).

and PPy/Fe_3O_4 nanocomposites primarily degrade between 245 and 450 °C, with the residual magnetic component remaining unchanged until 800 °C, indicating the desorption of bound water and the subsequent degradation of organic OA and PPy from the surface of the iron oxide particle. Two derivative peaks can be observed in the TGA curve for OA−Fe_3O_4 nanoparticles (Figure 4a). The first mass loss of 10% up to 280 °C is due to the degradation of weakly bound OA and adsorbed moisture. The second mass loss of 18% that appears between 300 and 350 °C corresponds to the loss of the covalently bonded OA molecules.[39] The TG thermogram of Fe_3O_4/PPy nanocomposites also shows two mass loss regions but at different temperature zones (Figure 4b), with the primary one in the range 300−400 °C representing the

https://doi.org/10.1021/acsomega.3c09864
ACS Omega 2024, 9, 19077−19088

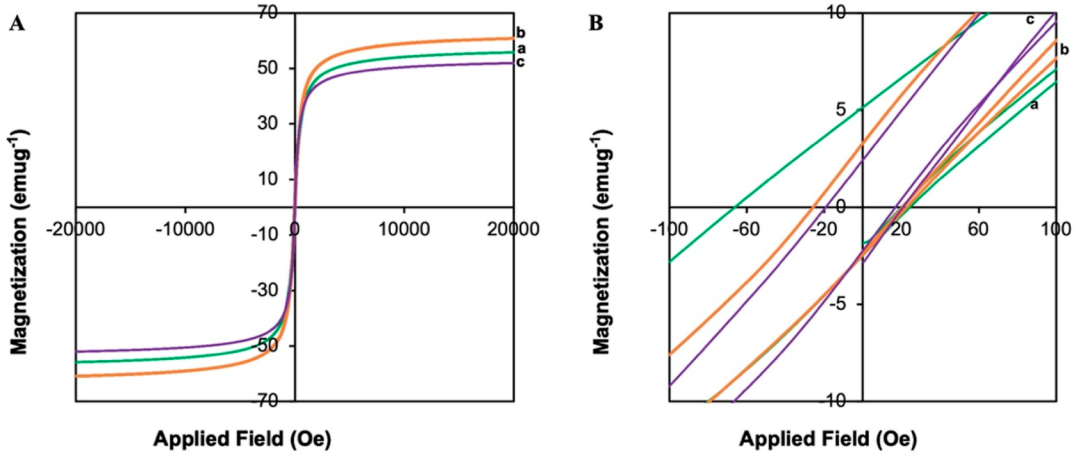

Figure 5. (A) Magnetization curves at 300 K for (a) OA−Fe_3O_4, (b) AA−Fe_3O_4, and (iii) PPy/Fe_3O_4 nanocomposites. (B) Magnetization curves at the low magnetic field region.

degradation of the PPy chain. The amount of residual PPy content in the PPy/Fe_3O_4 nanocomposites is estimated to be roughly 46% based on the organic component's full breakdown in the temperature range seen here. This outcome once more validates the Fe_3O_4 surface coating with the PPy polymer. It is important that the higher percentage (46%) of PPy as compared to OA coating (18%) is immobilized on the surface of the iron oxide nanoparticles.

The magnetic hysteresis curves for OA−Fe_3O_4, AA−Fe_3O_4 and PPy/Fe_3O_4 nanoparticles using VSM are shown in Figure 5A,B. The saturation magnetization (M_s) of OA−Fe_3O_4 nanoparticles [Figure 5A(a)] is ∼55.7 emu g^{-1} with very low coercivity (H_c) and remanence magnetization [Figure 5B(a)] observed, indicating the superparamagnetic nature. However, the saturation magnetization of AA−Fe_3O_4 [Figure 5A(b)] increased to 60 $emug^{-1}$, perhaps due to the breakdown of the OA chain into AA, resulting in the alteration of the surface property of the AA−Fe_3O_4 nanoparticles. Following functionalization of PPy, the saturation magnetization (M_s) is reduced to 52.0 emu g^{-1} [Figure 5A(c)] due to the subsequent formation of the thick conducting nonmagnetic PPy layer. The particles showed the traditional "*S*" shaped curve which indicates superparamagnetic behavior without hysteresis.[40] Consequently, it can be said that PPy/Fe_3O_4 nanocomposites possess the magnetic-responsive properties required for magnetic separation.

3.2. Adsorption of Cr (VI) Ions by PPy/Fe_3O_4 Nanocomposites. In this work, Cr (VI) ions were extracted from the aqueous medium using produced PPy/Fe_3O_4 nanocomposites as an adsorbent. The pH-dependent adsorption experiment, which is depicted in Figure 6, was carried out to optimize the pH condition. In the pH range 2−4, the amplitude of adsorption reached its maximum value of 83.59 mg g^{-1} with an adsorption efficiency of 90%. But when the pH rose, the values dropped precipitously, and at pH 8 and above, they were only 37 mg g^{-1} with 40% adsorption effectiveness.

3.3. Adsorption Mechanism. Adsorption of Cr ions either in the form of Cr (VI) or Cr (III) is mainly affected by pH value, which regulates the surface properties of Fe_3O_4/PPy nanocomposites and Cr ion species. The higher adsorption at lower pH values at which the nitrogen atom of the PPy chain becomes protonated and results anion exchange property of PPy with the monovalent bichromate ($HCrO_4^-$) and divalent dichromate ($Cr_2O_7^{2-}$) ions, as shown in Scheme 2.[41]

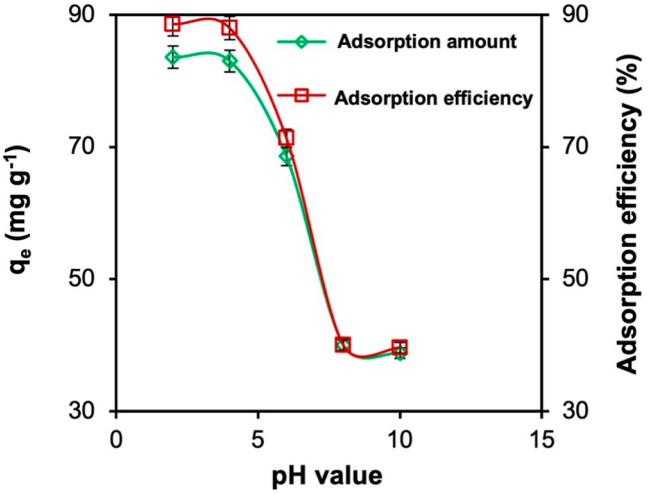

Figure 6. Impact of starting pH on the quantity and effectiveness of Cr(VI) ion adsorption on PPy/Fe_3O_4 nanocomposites. Condition: Cr(VI) ions, 25 mg L^{-1}; solid particle, 0.005 g; contact time, 120 min; total volume, 20 mL; temperature, 298 K.

Chromate (CrO_4^{2-}) ions are the predominant species at pH values greater than 6, and the concentration of hydroxide (OH^-) ions rises with increasing pH. Due to the charge density of the OH^- ion compared to the chromate ion's, sorption sites on composite particles are bonded to the hydroxide (OH^-) groups. As a result, some sorption sites are blocked for the chromate ion for the ion-exchange reactions.[42] It is also known that changes in pH can have an impact on PPy's chemical structure. Under acidic conditions, the Ppy polymer exists as a protonated salt, which is favorable for an anion-exchange reaction. However, when the pH value is increased, PPy becomes deprotonated or dedoped, a condition that is not favorable for an anion-exchange reaction. Beside the electrostatic interaction, additionally, there might be other ways for Cr (VI) ions to be ingested as Cr (III), which is produced when Cr(VI) is reduced at an acidic pH and complexes with PPy polymer chains that are present on Fe_3O_4 nanoparticles.[43,44] Therefore, considering these potential factors, further experiments in this adsorption study were conducted at pH 2. Though some Cr(III) species adsorbed by coordination interaction may still be present on the nano-

https://doi.org/10.1021/acsomega.3c09864
ACS Omega 2024, 9, 19077−19088

Scheme 2. Schematic Illustration for the Adsorption of Chromium (Cr) Ions via Formation of $HCrO_4^-$ Ions, which Displaces the Cl^- Ions on PPy of the Magnetic Nanocomposites

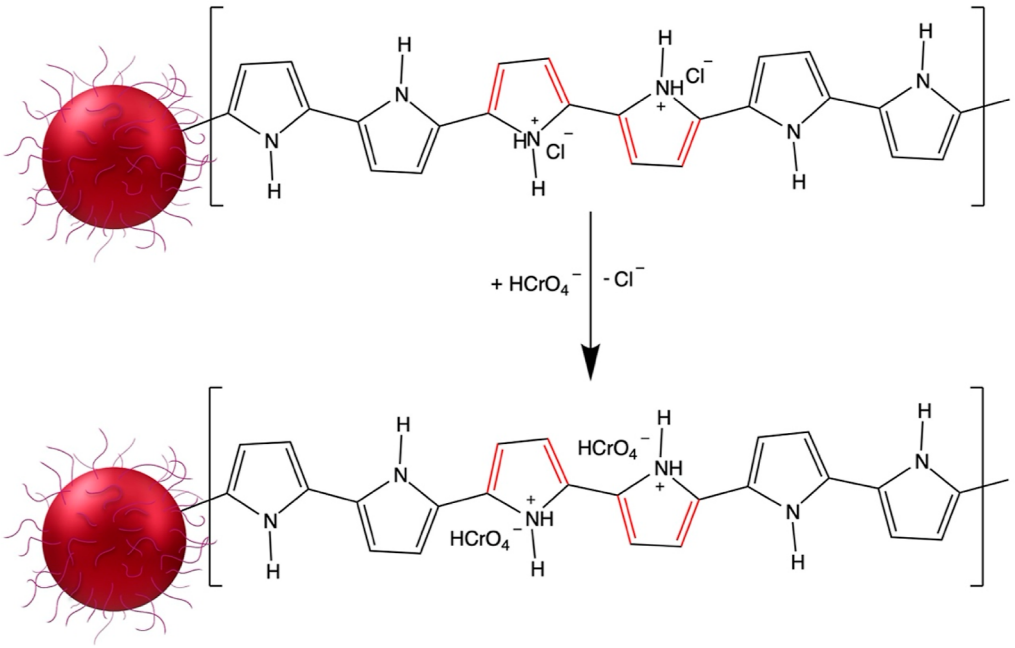

composites, $HCrO_4^-$ ions adsorbed via electrostatic attraction were desorbable with a NaOH solution.

Figure 7 shows the contact-time-dependent adsorption behavior conducted to monitor the rate of adsorption and

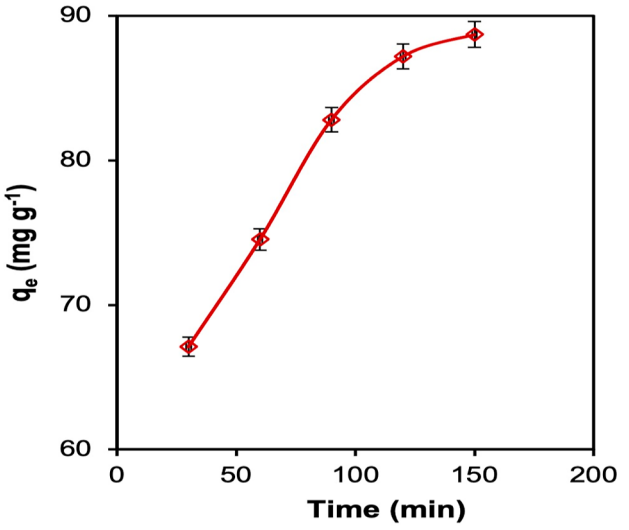

Figure 7. Impact of the duration of contact time on Cr(VI) ions on PPy/Fe_3O_4 nanocomposites. Conditions: Cr (VI), 25 mg L^{-1}; solid, 0.005 g; volume, 20 mL; temperature, 298 K; pH 2.

evaluate the time for maximum Cr(VI) separation. Initially, the Cr(VI) adsorption rate increases until almost reaching a steady state after 120 min. The increased concentration of Cr(VI) ions and more free active sites on the nanocomposite particles are the reasons of the initial high adsorption rate.

Figure 8 illustrates the adsorption behavior as a function of the temperature and initial Cr (VI) ion concentration. Independent of temperature, the amount of adsorption increases with the initial concentration of Cr(VI) ions. A

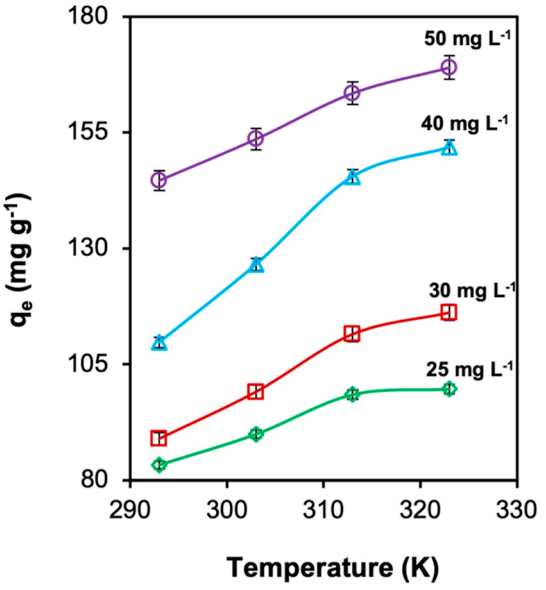

Figure 8. Adsorption behavior of Cr(VI) on PPy/Fe_3O_4 nanocomposites: Initial Cr(VI) concentration was dependent as a function of temperature.

higher chance of collision between Cr(VI) ions and the PPy/Fe_3O_4 nanocomposite surfaces is thought to be caused by the higher concentration of Cr(VI) ions acting as a driving force that overcomes the mass transfer resistance of the Cr(VI) ions between the aqueous and solid phases. An increase in temperature increases the anion exchange between the chromate ion and the dopant group of PPy/Fe_3O_4 nanocomposite particles, indicating an endothermic adsorption process. Table 1 shows a comparison of the adsorption of Cr(VI) ions with various adsorbents documented in the literature using the magnetic nanocomposites prepared here.

https://doi.org/10.1021/acsomega.3c09864
ACS Omega 2024, 9, 19077−19088

Table 1. Comparison Data for Maximum Adsorption (mg g^{-1}) of Cr(VI) Ions by Iron Oxide-Based Magnetic Nanocomposites

adsorbent materials	maximum adsorption capacity (mg g^{-1})	References
bare Fe_3O_4	3.56	45
Fe_3O_4/PPy	119	46
montmorillonite-supported magnetite nanoparticles	15.3	47
porous magnetite nanoparticles	14.49	48
humic acid coated nanoparticle	24.13	49
magnetic gelatin	106.38	50
glycine doped PPy magnetic nanocomposite	238−303	51
Fe_3O_4/PPy	170	this work

3.4. Adsorption Isotherms. Adsorption isotherms are useful for confirming the interaction between the adsorbate and adsorbent molecules, providing information about the sorption mechanism as well as the surface structure of the interacting materials. The three most used isotherm models—Langmuir, Freundlich, and Temkin (Figure 9) were applied in this study to examine Cr(VI) adsorption behavior on PPy/Fe_3O_4 nanocomposite particles. Table 2 lists the various

Table 2. Adsorption Isotherm Parameters of the Langmuir, Freundlich, and Temkin Models

isotherm equation		303 K	313 K	323 K
Langmuir constants	q_{max} (mg g^{-1})	170.99	171.52	173.22
	b (L mg^{-1})	0.570	2.216	7.326
	R^2	0.9804	0.9987	0.9997
	R_L	0.034	0.009	0.0027
Freundlich constants	$1/n$	0.2941	0.2054	0.1336
	K_f (mg g^{-1})	63.857	102.024	138.488
	R^2	0.7391	0.7345	0.9827
Temkin constants	A_T (L mg^{-1})	2.6739	188.669	309.3
	b_T	44.134	22.292	17.57
	R^2	0.9939	0.9919	0.9892

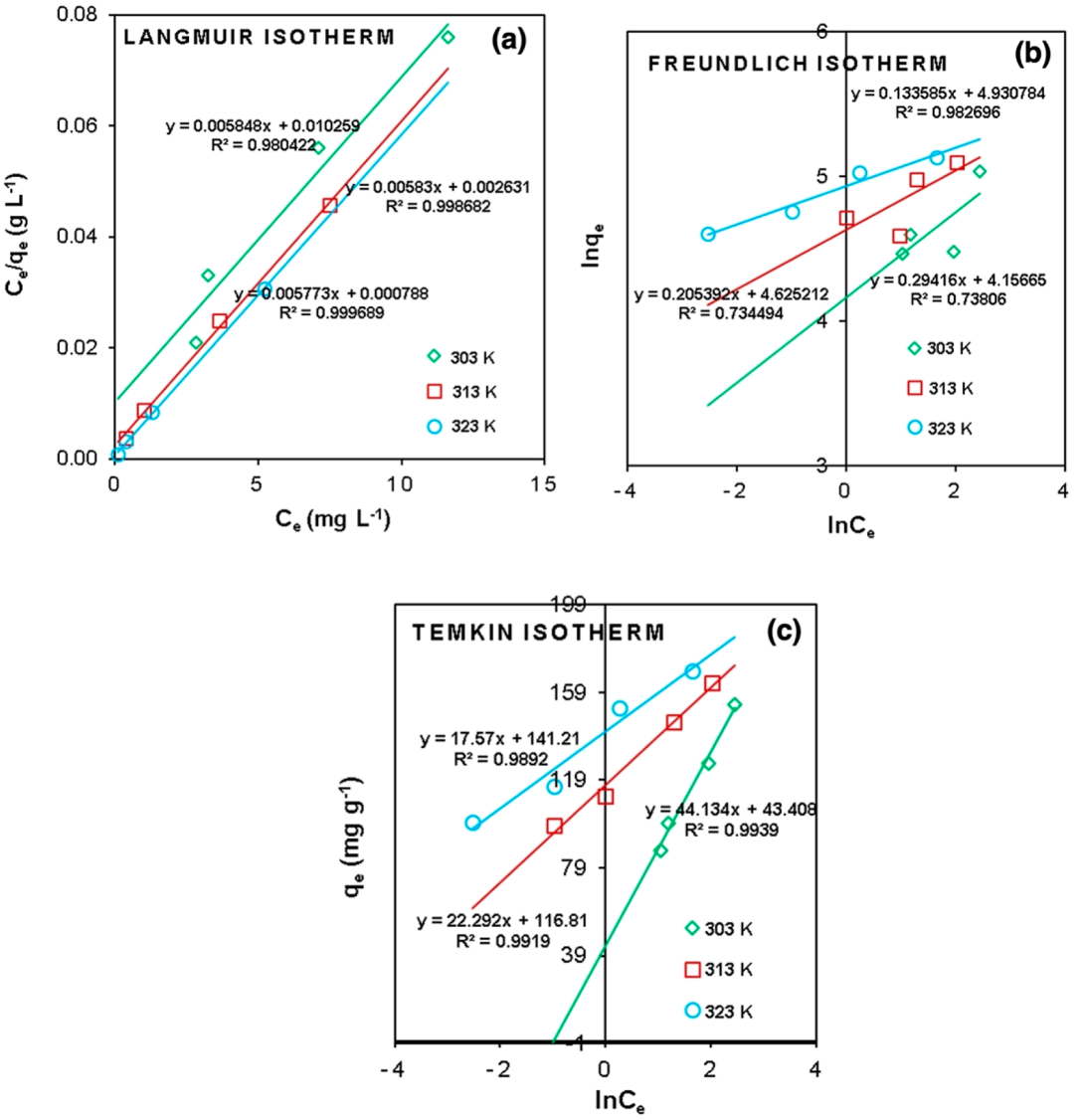

Figure 9. Different adsorption isotherm models for Cr(VI) adsorption on PPy/Fe_3O_4 nanocomposites: (a) Langmuir, (b) Freundlich, and (c) Temkin.

https://doi.org/10.1021/acsomega.3c09864
ACS Omega 2024, 9, 19077−19088

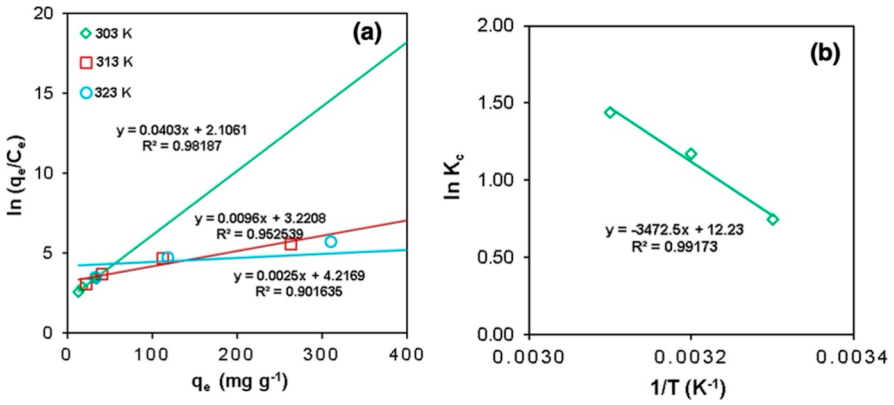

Figure 10. (a) Plots of $\ln(q_e/C_e)$ versus q_e for the determination of adsorption equilibrium constant K_c, and (b) Van't Hoff plot of adsorption equilibrium constant K_c.

empirical constants that were determined by analyzing the slopes and intercepts of the three linear isotherm plots. Considering the best correlation coefficient (R^2, 0.9997), the Langmuir model is the most suitable adsorption isotherm, as indicated by the data in the table. This finding suggests that adsorption occurs in a monolayer mode as opposed to a multilayer structure, and that the adsorbent surfaces are uniformly distributed and homogeneous.

The heat of adsorption, which does not depend on the number of active sites on the PPy/Fe_3O_4 nanocomposites, is equal for all active sites; further, there are no interactions among the Cr(VI) ions. The fact that q_{max} increases as temperature rises indicates that the adsorption process is endothermic, and it is advantageous since the constant (R_L) falls between zero and unity. The dimensionless constant ($1/n$) calculated from Freundlich's linear isotherm curve is less than unity, also confirming that the adsorption process is favorable. The equilibrium binding constant (A_T) calculated from the Temkin model isotherm equation shows a maximum value of 3093 L mg^{-1} at 323 K temperature. This result supports the strong interaction between the Cr(VI) ions and PPy/Fe_3O_4 nanocomposite particles. The synthesized nanocomposites can be an effective adsorbent for the anion-exchange separation of heavy metal ions from contaminated water, according to this adsorption study.

3.5. Thermodynamic Parameters. The linear plot of $\ln(q_e/C_e)$ against q_e (Figure 10a) is used to compute the thermodynamic equilibrium constant (K_c), the values of which are listed in Table 3. The magnitude of K_c increases with temperature rise, becoming double for only an increase of 20 °C, indicating the prepared PPy/Fe_3O_4 nanocomposite particles exhibit a higher Cr (VI) ion removal at higher temperatures. Equation 6 was utilized to calculate the variation in free energy (ΔG), and the linear form of the Van't Hoff eq (Figure 10b) was used to figure out the changes in entropy (ΔS) and enthalpy (ΔH). The calculated ΔH value is +28.87 kJ mol^{-1} and lies in the range from +20.9 to +418.4 kJ mol^{-1}. Once more, the positive value implies that the adsorption process is endothermic and could possibly be chemisorption.[52,53] The adsorption process is thermodynamically favorable, as confirmed by the negative value of $\Delta G°$. Though the negative Delta value does not indicate the spontaneous adsorption process.[54] Without taking into account the sign, the magnitude of $\Delta G°$ grows as the temperature rises, further indicating that the Cr(VI) sorption process is favorable at higher temperatures. The comparatively high, positive $\Delta S°$ value, 101.68 J mol^{-1} K^{-1} implies the increased randomness at the solid−solute interface during the adsorption process indicating higher Cr(VI) ion adsorption on Fe_3O_4/PPy nanocomposites.[55]

Table 3. Cr(VI) Adsorption Equilibrium Constant and Thermodynamic Characteristics on the PPy/Fe_3O_4 Nanocomposite

	temperature (K)		
thermodynamic constants	303	313	323
K_c	2.1061	3.2208	4.2169
$\Delta G°$ (kJ/mol)	−1.939	−2.9558	−3.9726
$\Delta H°$ (kJ/mol)	+28.87		
$\Delta S°$ (J mol^{-1} K^{-1})	+101.68		

3.6. Sorption Kinetics Study. To investigate the mechanism and the steps controlling the rate controlling involved in the adsorption process, the experimental data from the time-dependent adsorption investigation at 298 K was tested using pseudo-first-order and pseudo-second-order kinetic models (Figure 7). The following Lagergren rate equation yields the pseudo-first-order kinetic equation[56,57]

$$\log(q_e - q_t) = \log q_e - (k_1/2.303) \times t \quad (7)$$

where q_t (mg g^{-1}) is the amount of Cr(VI) adsorbed on the surface of the PPy/Fe_3O_4 nanocomposite particles at time t, q_e (mg g^{-1}) is the adsorption capacity at equilibrium, and k_1 (min^{-1}) is the equilibrium rate constant of the pseudo-first-order adsorption. In Figure 11a, the plot of $\log(q_e - q_t)$ against t gives the value of $\log q_e$ from the intercept. The value of k_1 calculated from the linear graph is equal to 0.009 min^{-1}. The q_e value obtained from the Lagergren plot is 42.58 mg g^{-1}, a value much different from the experimental q_e value (83.59 mg g^{-1}), meaning the pseudo-first-order kinetics is less likely to explain the rate processes.

The equation of the pseudo-second-order kinetic model proposed by Ritchie is as follows

$$t/q_t = 1/k_2 q_{max}^2 + (1/q_{max})t \quad (8)$$

where k_2 (mg g^{-1} min^{-1}) is the equilibrium rate constant. According to the Ritchie pseudo-second-order equation, a plot of t/q_t against t (Figure 11b) gives $1/q_e$ from the slope and k_2 from the intercept. The theoretical q_e value estimated from the pseudo-second-order kinetics of 100 mg g^{-1} agrees well with

https://doi.org/10.1021/acsomega.3c09864
ACS Omega 2024, 9, 19077−19088

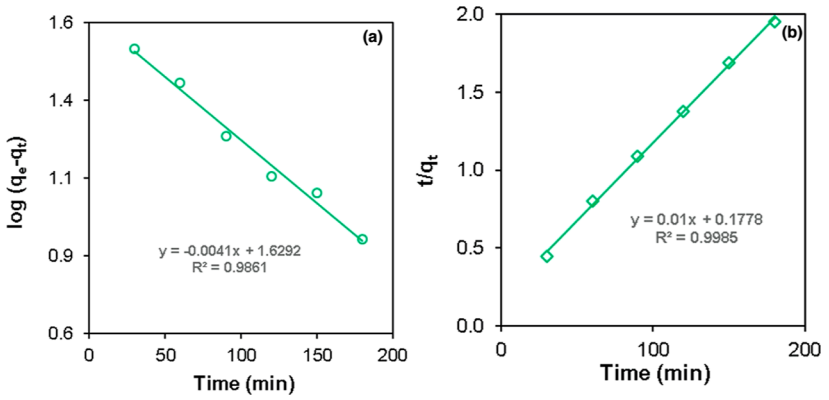

Figure 11. Kinetic plots for the adsorption of Cr(VI) on PPy/Fe_3O_4 composite particles: (a) Lagergren pseudo-first-order model and (b) pseudo-second-order model.

the experimental value (89.96 mg g^{-1}). The calculated correlation coefficients are also closer to unity (R^2 = 0.99) for the pseudo-second-order kinetics than for the pseudo-first-order kinetics (R^2 = 0.98) model. This finding clearly implies that chemisorption was the primary process controlling the adsorption of Cr(VI) on the PPy/Fe_3O_4 nanocomposites and that the adsorption process followed a pseudo-second-order rate process.

3.7. Reusability of PPy/Fe_3O_4 Nanocomposites. The recycling and reuse of any adsorbent material is in top demand for industrial applications as well as for reducing the cost. To monitor the reusability of prepared PPy/Fe_3O_4 nanocomposite particles, a series of adsorption and desorption experiments were conducted, with the results shown in Figure 12. Cr(VI)-adsorbed magnetic nanocomposites were subjected to a desorption experiment before reuse. The addition of a base NaOH solution to the Cr(VI)-loaded adsorbent increases the pH and induces the release of Cr(VI) ions to dispersion medium. It was found that there was no desorption in neutral and acidic pH while it occurred at alkaline conditions, indicating electrostatic adsorption onto magnetic nanocomposites. In the first cycle, the Cr(VI) removal efficiency is almost 90%. But after each cycle, the value is gradually decreased, and after the fifth cycle becomes 54%. The successive decrease in adsorption might be based on the loss of the adsorbent particles during the repeated recovery and application processes.

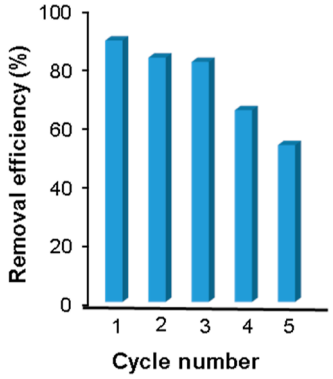

Figure 12. Correlation between regeneration cycles and the percentage of Cr(VI) ions removed by PPy/Fe_3O_4 nanocomposites.

4. CONCLUSIONS

In summary, this research successfully prepared conducting PPy coated magnetite nanocomposites (PPy/Fe_3O_4) via the Lemieux-von Rudloff oxidation of OA-Fe3O4 nanoparticles. The nanocomposite PPy/Fe_3O_4 has a comparatively high value of magnetic saturation (M_s) provided that the nanocomposites were magnetically recoverable adsorbent materials for the removal of Cr(VI) ions from a water sample through the ion-exchange mechanism. The maximum removal capacity for Cr(VI) ions was found to be 170 mg g^{-1} at pH 2, which induced the protonated imine group of PPy to interact electrostatically with the Cr(VI) anions. The Langmuir isotherm model was the most accurate to explain this adsorption process, according to the correlation coefficients of the Freundlich, Temkin, and Langmuir adsorption isotherms. The adsorption process is endothermic and favorable at a high temperature; the negative value of the Gibbs free energy confirmed that the sorption process is spontaneous. A pseudo-second-order kinetic model was fitted with the kinetic data, and the theoretical adsorption capacity was found to be equal to the experimental adsorption capacity value. Adsorbent materials could be used multiple times for the removal of Cr(VI) ions with only a small decrease in removal efficiency with respect to the amount of adsorbed Cr(VI) ions reported in the literature. As a result, it can be concluded that PPy/Fe_3O_4 composite particles can be successfully used as an adsorbent for toxic heavy metals in polluted water.

AUTHOR INFORMATION

Corresponding Author

Md. Mahbubor Rahman − *Polymer Colloids & Nanomaterials Group, Department of Chemistry, Faculty of Science, University of Rajshahi, Rajshahi 6205, Bangladesh; Department of Materials Science & Engineering, Clemson University, Clemson, South Carolina 29634-0971, United States;* orcid.org/0000-0002-6763-525X; Phone: +88-02588864107; Email: mrchem@ru.ac.bd; Fax: +88-02588866364

Authors

Md. Kawsar Hossain − *Department of Chemistry, Pabna University of Science and Technology, Pabna 6600, Bangladesh*

Md. Mehadi Hasan − *Polymer Colloids & Nanomaterials Group, Department of Chemistry, Faculty of Science, University of Rajshahi, Rajshahi 6205, Bangladesh*

https://doi.org/10.1021/acsomega.3c09864
ACS Omega 2024, 9, 19077−19088

Md. Shahidul Islam − *Polymer Colloids & Nanomaterials Group, Department of Chemistry, Faculty of Science, University of Rajshahi, Rajshahi 6205, Bangladesh*

O. Thompson Mefford − *Department of Materials Science & Engineering, Clemson University, Clemson, South Carolina 29634-0971, United States;* orcid.org/0000-0002-9164-2521

Hasan Ahmad − *Polymer Colloids & Nanomaterials Group, Department of Chemistry, Faculty of Science, University of Rajshahi, Rajshahi 6205, Bangladesh;* orcid.org/0000-0003-1499-167X

Complete contact information is available at: https://pubs.acs.org/10.1021/acsomega.3c09864

Notes

The authors declare no competing financial interest.

■ ACKNOWLEDGMENTS

The authors acknowledge the University Grants Commission (UGC) Dhaka, Ministry of Science & Technology, Bangladesh and Faculty of Science, University of Rajshahi for financial support.

■ REFERENCES

(1) Nargis, A.; Habib, A.; Islam, M. N.; Chen, K.; Sarker, M. S. I.; Al-Razee, A. N. M.; Liu, W.; Liu, G.; Cai, M. Source identification, contamination status and health risk assessment of heavy metals from road dusts in Dhaka, Bangladesh. *J. Environ. Sci.* **2022**, *121*, 159−174.

(2) Gan, Y.; Miao, Y.; Wang, L.; Yang, G.; Li, Y. C.; Wang, W.; Dai, J. Source contribution analysis and collaborative assessment of heavy metals in vegetable-growing soils. *J. Agric. Food Chem.* **2018**, *66*, 10943−10951.

(3) Zou, Y.; Wang, X.; Khan, A.; Wang, P.; Liu, Y.; Alsaedi, A.; Hayat, T.; Wang, X. Environmental remediation and application of nanoscale zero-valent iron and its composites for the removal of heavy metal ions: a review. *Environ. Sci. Technol.* **2016**, *50*, 7290−7304.

(4) Zhitkovich, A. Chromium in drinking water: sources, metabolism, and cancer risks. *Chem. Res. Toxicol.* **2011**, *24*, 1617−1629.

(5) Cheung, K. H.; Gu, J. D. Mechanism of hexavalent chromium detoxification by microorganisms and bioremediation application potential: a review. *Int. Biodeterior. Biodegrad.* **2007**, *59*, 8−15.

(6) Jin, W.; Zhang, Y. Sustainable electrochemical extraction of metal resources from waste streams: from removal to recovery. *ACS Sustainable Chem. Eng.* **2020**, *8*, 4693−4707.

(7) Polat, H.; Erdogan, D. Heavy metal removal from waste waters by ion flotation. *J. Hazard. Mater.* **2007**, *148*, 267−273.

(8) Shen, L. C.; Nguyen, X. T.; Hankins, N. P. Removal of heavy metal ions from dilute aqueous solutions by polymer-surfactant aggregates: a novel effluent treatment process. *Sep. Purif. Technol.* **2015**, *152*, 101−107.

(9) Zhu, W. P.; Sun, S. P.; Gao, J.; Fu, F. J.; Chung, T. S. Dual layer polybenzimidazole/polyethersulfone (PBI/PES) nanofiltration (NF) hollow fiber membranes for heavy metals removal from wastewater. *J. Membr. Sci.* **2014**, *456*, 117−127.

(10) Sardella, F.; Gimenez, M.; Navas, C.; Morandi, C.; Deiana, C.; Sapag, K. Conversion of viticultural industry wastes into activated carbons for removal of lead and cadmium. *J. Environ. Chem. Eng.* **2015**, *3*, 253−260.

(11) Ihsanullah, F. A.; Al-Khaldi, F. A.; Abusharkh, B.; Khaled, M.; Atieh, M. A.; Nasser, M. S.; laoui, T.; Saleh, T. A.; Agarwal, S.; Tyagi, I.; et al. Adsorptive removal of cadmium (II) ions from liquid phase using acid modified carbon-based adsorbents. *J. Mol. Liq.* **2015**, *204*, 255−263.

(12) Pan, B.; Pan, B.; Zhang, W.; Lv, L.; Zhang, Q.; Zheng, S. Development of polymeric and polymer-based hybrid adsorbents for pollutants removal from waters. *Chem. Eng. J.* **2009**, *151*, 19−29.

(13) Zhao, G.; Wu, X.; Tan, X.; Wang, X. Sorption of heavy metal ions from aqueous solutions: A review. *Open Colloid Sci. J.* **2011**, *4*, 19−31.

(14) Zhang, R.; Ma, H.; Wang, B. Removal of chromium (VI) from aqueous solutions using polyaniline doped with sulfuric acid. *Ind. Eng. Chem. Res.* **2010**, *49*, 9998−10004.

(15) Karthik, R.; Meenakshi, S. J. Removal of hexavalent chromium ions using polyaniline/silica gel composite. *Water Proc. Eng.* **2014**, *1*, 37−45.

(16) Qiu, B.; Xu, C.; Sun, D.; Wang, Q.; Gu, H.; Zhang, X.; Weeks, B. L.; Hopper, J.; Ho, T. C.; Guo, Z.; Wei, S. Polyaniline coating with various substrates for hexavalent chromium removal. *Appl. Surf. Sci.* **2015**, *334*, 7−14.

(17) Zheng, Y.; Wang, W.; Huang, D.; Wang, A. Kapok fiber oriented-polyaniline nanofibers for efficient Cr(VI) removal. *Chem. Eng. J.* **2012**, *191*, 154−161.

(18) Ahmad, H.; Rahman, M. M.; Ali, M. A.; Minami, H.; Tauer, K.; Gafur, M. A.; Rahman, M. M. A simple route to synthesize conductive stimuli-responsive polypyrrole nanocomposite hydrogel particles with strong magnetic properties and their performance for removal of hexavalent chromium ions from aqueous solution. *J. Magn. Magn. Mater.* **2016**, *412*, 15−22.

(19) Zayan, S.; Elshazly, A.; Elkady, M. In situ polymerization of polypyrrole@aluminum fumarate metal-organic framework hybrid nanocomposites for the application of wastewater treatment. *Polymers* **2020**, *12*, 1764.

(20) Ansari, R.; Fahim, N. K. Application of polypyrrole coated on wood sawdust for removal of Cr(VI) ion from aqueous solutions. *React. Funct. Polym.* **2007**, *67*, 367−374.

(21) Choi, M.; Jang, J. Heavy metal ion adsorption onto polypyrrole-impregnated porous carbon. *J. Colloid Interface Sci.* **2008**, *325*, 287−289.

(22) Tang, S. C. N.; Yan, D. Y. S.; Lo, I. M. C. Sustainable wastewater treatment using microsized magnetic hydrogel with magnetic separation technology. *Ind. Eng. Chem. Res.* **2014**, *53*, 15718−15724.

(23) Zhu, K.; Chen, C.; Xu, H.; Gao, Y.; Tan, X.; Alsaedi, A.; Hayat, T. Cr(VI) reduction and immobilization by core-double-shell structured magnetic polydopamine@zeoliticidazolate frameworks-8 microspheres. *ACS Sustain. Chem. Eng.* **2017**, *5*, 6795−6802.

(24) Yu, Z.; Zhang, X.; Huang, Y. Magnetic chitosan-iron (iii) hydrogel as a fast and reusable adsorbent for chromium (vi) removal. *Ind. Eng. Chem. Res.* **2013**, *52*, 11956−11966.

(25) Huang, J.; Cao, Y.; Shao, Q.; Peng, X.; Guo, Z. Magnetic nanocarbon adsorbents with enhanced hexavalent chromium removal: morphology dependence of fibrillar vs particulate structures. *Ind. Eng. Chem. Res.* **2017**, *56*, 10689−10701.

(26) Wan, C.; Li, J. Facile synthesis of well-dispersed super-paramagnetic γ-fe$_2$o$_3$ nanoparticles encapsulated in three-dimensional architectures of cellulose aerogels and their applications for cr(vi) removal from contaminated water. *ACS Sustain. Chem. Eng.* **2015**, *3*, 2142−2152.

(27) Wei, C.; German, S.; Basak, S.; Rajeshwar, K. Reduction of hexavalent chromium in aqueous solutions by polypyrrole. *J. Electrochem. Soc.* **1993**, *140*, L60−L62.

(28) Chávez-Guajardo, A. E.; Medina-Llamas, J. C.; Maqueira, L.; Andrade, C. A. S.; Alves, K. G. B.; de Melo, C. P. Efficient removal of Cr(VI) and Cu(II) ions from aqueous media by use of polypyrrole/maghemite and polyaniline/maghemite magnetic nanocomposites. *Chem. Eng. J.* **2015**, *281*, 826−836.

(29) Ahmad, H.; Rahman, M. M.; Ali, M. A.; Minami, H.; Tauer, K.; Gafur, M. A.; Rahman, M. M. A simple route to synthesize conductive stimuli-responsive polypyrrole nanocomposite hydrogel particles with strong magnetic properties and their performance for removal of hexavalent chromium ions from aqueous solution. *J. Magn. Magn. Mater.* **2016**, *412*, 15−22.

(30) Chen, Z.; Chen, H.; Hu, H.; Yu, M.; Li, F.; Zhang, Q.; Zhou, Z.; Yi, T.; Huang, C. Versatile synthesis strategy for carboxylic acid-functionalized upconverting nanophosphors as biological labels. *J. Am. Chem. Soc.* **2008**, *130*, 3023−3029.
(31) Bithi, K. A.; Minami, H.; Hossain, M. K.; Rahman, M. M.; Rahman, M. A.; Gafur, M. A.; Ahmad, H. Cationic polyelectrolyte grafted mesoporous magnetic silica composite particles for targeted drug delivery and thrombolysis. *Materialia* **2020**, *11*, 100676.
(32) Hossain, M. K.; Minami, H.; Hoque, S. M.; Rahman, M. M.; Sharafat, M. K.; Begum, M. F.; Islam, M. E.; Ahmad, H. Mesoporous electromagnetic composite particles: electric current responsive release of biologically active molecules and antibacterial properties. *Colloids Surf., B* **2019**, *181*, 85−93.
(33) Kim, K. D.; Kim, S. S.; Choa, Y. H.; Kim, H. T. Formation and surface modification of Fe_3O_4 nanoparticles by co-precipitation and sol-gel method. *J. Ind. Eng. Chem.* **2007**, *13*, 1137−1141.
(34) Patil, R. M.; Shete, P. B.; Thorat, N. D.; Otari, S. V.; Barick, K. C.; Prasad, A.; Ningthoujam, R. S.; Tiwale, B. M.; Pawar, S. H. Non-aqueous to aqueous phase transfer of oleic acid coated iron oxide nanoparticles for hyperthermia application. *RSC Adv.* **2014**, *4*, 4515−4522.
(35) Zhang, L.; He, R.; Gu, H.-C. Oleic acid coating on the monodisperse magnetite nanoparticles. *Appl. Surf. Sci.* **2006**, *253*, 2611−2617.
(36) Jang, J.; Oh, J. Fabrication of a highly transparent conductive thin film from polypyrrole/poly (methyl methacrylate) core/shell nanospheres. *Adv. Funct. Mater.* **2005**, *15*, 494−502.
(37) Romero, A. J. F.; Cascales, J. J. L.; Otero, T. F. In situ FTIR spectroscopy study of the breakin phenomenon observed for PPy/PVS films in acetonitrile. *J. Phys. Chem. B* **2005**, *109*, 21078−21085.
(38) Liu, F.; Yuan, Y.; Li, L.; Shang, S.; Yu, X.; Zhang, Q.; Jiang, S.; Wu, Y. Synthesis of polypyrrole nanocomposites decorated with silver nanoparticles with electrocatalysis and antibacterial property. *Composites, Part B* **2015**, *69*, 232−236.
(39) Kandori, K.; Ishikawa, T. TPD-MS-TG study of hematite particles produced by the forced hydrolysis reaction. *Phys. Chem. Chem. Phys.* **2001**, *3*, 2949−2954.
(40) Cai, J.; Guo, J.; Ji, M.; Yang, W.; Wang, C.; Fu, S. Preparation and characterization of multi-responsive polymer composite microspheres with core-shell structure. *Colloid Polym. Sci.* **2007**, *285*, 1607−1615.
(41) Wang, K.; Qiu, G.; Cao, H.; Jin, R. Removal of chromium (vi) from aqueous solutions using Fe_3O_4 magnetic polymer microspheres functionalized with amino groups. *Materials* **2015**, *8*, 8378−8391.
(42) Shen, H.; Chen, J.; Dai, H.; Wang, L.; Hu, M.; Xia, Q. New insights into the sorption and detoxification of chromium(vi) by tetraethylenepentamine functionalized nanosized magnetic polymer adsorbents: mechanism and pH effect. *Ind. Eng. Chem. Res.* **2013**, *52*, 12723−12732.
(43) Cui, J.; Li, X.; Ma, S.; Wei, W. Cellulose bridged carbonate hydroxyapatite nanoparticles as novel adsorbents for efficient Cr(VI) removal. *J. Dispersion Sci. Technol.* **2023**, *44*, 2711−2722.
(44) Bhaumik, M.; Maity, A.; Srinivasu, V. V.; Onyango, M. S. Enhanced removal of Cr(VI) from aqueous solution using polypyrrole/ Fe_3O_4 magnetic nanocomposite. *J. Hazard. Mater.* **2011**, *190*, 381−390.
(45) Sharma, C.; Srivastava, V. Comparative studies of removal of Cr(VI) and Ni(II) from aqueous solutions by magnetic nanoparticles. *J. Chem. Eng. Data* **2011**, *56*, 819−825.
(46) Muliwa, A. M.; Leswifi, T. Y.; Onyango, M. S.; Maity, A. Magnetic adsorption separation (MAS) process: An alternative method of extracting Cr(VI) from aqueous solution using polypyrrole coated Fe3O4 nanocomposites. *Sep. Purif. Technol.* **2016**, *158*, 250−258.
(47) Yuan, P.; Fan, M.; Yang, D.; He, H.; Liu, D.; Yuan, A.; Zhu, J. X.; Chen, T. H. Montmorillonite-supported magnetite nanoparticles for the removal of hexavalent chromium [Cr(VI)] from aqueous solutions. *J. Hazard. Mater.* **2009**, *166*, 821−829.
(48) Ren, G.; Wang, X.; Huang, P.; Zhong, B.; Zhang, Z.; Yang, L.; Yang, X. Chromium (VI) adsorption from wastewater using porous magnetite nanoparticles prepared from titanium residue by a novel solid-phase reduction method. *Sci. Total Environ.* **2017**, *607−608*, 900−910.
(49) Singaraj, S. G.; Mahanty, B.; Balachandran, D.; Padmaprabha, A. Adsorption and desorption of chromium with humic acid coated iron oxide nanoparticles. *Environ. Sci. Pollut. Res.* **2019**, *26*, 30044−30054.
(50) Chen, G.; Qiao, C.; Wang, Y.; Yao, J. Synthesis of magnetic gelatin and its adsorption property for Cr(VI). *Ind. Eng. Chem. Res.* **2014**, *53*, 15576−15581.
(51) Ballav, N.; Choi, H. J.; Mishra, S. B.; Maity, A. Synthesis, characterization of Fe3O4@glycine doped polypyrrole magnetic nanocomposites and their potential performance to remove toxic Cr(VI). *J. Ind. Eng. Chem.* **2014**, *20*, 4085−4093.
(52) Xu, F.; Liu, X.; Chen, Y.; Zhang, K.; Xu, H. Self-assembly modified-mushroom nanocomposite for rapid removal of hexavalent chromium from aqueous solution with bubbling fluidized bed. *Sci. Rep.* **2016**, *6*, 26201.
(53) Karthik, R.; Meenakshi, S. Removal of Cr(VI) ions by adsorption onto sodium alginate-polyaniline nanofibers. *Int. J. Biol. Macromol.* **2015**, *72*, 711−717.
(54) Tran, H. N. Improper Estimation of Thermodynamic Parameters in Adsorption Studies with Distribution Coefficient K_D (q_e/C_e) or Freundlich Constant (K_F): Considerations from the Derivation of Dimensionless Thermodynamic Equilibrium Constant and Suggestions. *Adsorpt. Sci. Technol.* **2022**, *2022*, 5553212.
(55) Babaei, A. A.; Baboli, Z.; Jaafarzadeh, N.; Goudarzi, G.; Bahrami, M.; Ahmadi, M. Synthesis, performance, and nonlinear modeling of modified nano-sized magnetite for removal of Cr(VI) from aqueous solutions. *Desalin. Water Treat.* **2015**, *53*, 768−777.
(56) Tong, Z.; Zheng, P.; Bai, B.; Wang, H.; Suo, Y. Adsorption performance of methyl violet via α-Fe_2O_3@porous hollow carbonaceous microspheres and its effective regeneration through a fenton-like reaction. *Catalysts* **2016**, *6*, 58.
(57) Lagergren, S. About the theory of so-called adsorption of soluble substances. *K. Sven. Vetenskapsakad. Handl.* **1898**, *24*, 1−39.

https://doi.org/10.1021/acsomega.3c09864
ACS Omega 2024, 9, 19077−19088